Structural Evolution in Metal Oxide/Semiconductor Colloidal Nanocrystal Heterostructures

Kwan-Wook Kwon, Bo Hyun Lee, and Moonsub Shim*

Department of Materials Science and Engineering and Frederick Seitz Materials Research Laboratory, University of Illinois at Urbana−Champaign, Urbana, Illinois 61801

Received September 9, 2006. Revised Manuscript Received October 25, 2006

Colloidal nanocrystal heterostructures in which two or more chemically distinct inorganic components are epitaxially fused together provide new opportunities in developing multifunctional building block materials. The ability to synthesize structurally and chemically well-defined nanocrystal heterostructures can provide novel combinations of unique properties arising at the nanometer length scale. Here, we examine the structural evolution of inverse spinel iron oxide/CdS nanocrystal heterostructures with respect to the sizes of both components. The crystal structure and the crystallinity of the initial iron oxide are first identified by a combination of X-ray diffraction and Raman scattering measurements. Studies on the size effect suggest lattice-strain-induced limitations on the achievable sizes of CdS within the heterostructures. Because of this limitation, increasing the amount of Cd/S reagents leads to multiple particle nucleation on individual iron oxide nanocrystals rather than continued growth. Larger sizes and a limited amount of the CdS component can be achieved by starting with small iron oxide nanocrystals. These results suggest that exploiting lattice strain may be a viable approach to obtaining heterostructured colloids with nanoscale precision.

Introduction

Colloidal nanocrystal (NC) heterostructures[1] consisting of two or more inorganic phases provide novel approaches in engineering materials' properties. A variety of unique aspects arising at the nanometer length scale from enormous surface areas to quantum-confinement effects may be combined to achieve unprecedented multifunctional capabilities. For example, simultaneously achievable magnetically directed motion and fluorescence imaging with heterostructured NCs may find use in biomedical applications.[2] Intricate ordered structures may be realized by a combination of electrically, magnetically, and/or chemically directed assemblies.[3] Wavelength tunable photovoltaic and photocatalytic materials with efficient charge separation capabilities may also be achieved with heterostructures incorporating semiconductor NCs with size-tunable optical properties.[4] To synthesize structurally and chemically well-defined heterostructured NC colloids with which many breakthrough technologies may be envisioned, it is necessary to have an in-depth understanding of how interfaces form at the nanometer length scale.

In synthesizing both core/shell and anisotropic (e.g., dimers, trimers, etc., of two or more types of materials) colloidal NC heterostructures, the first key requirement is preventing separate homogeneous nucleation of the second inorganic phase. To promote nucleation of the second phase on the surfaces of the first phase, the surface capping molecules should not be bound too strongly such that they interfere with the heterointerface formation and the interfacial chemistry of the two phases must be compatible. Especially in crystalline systems, interfacial strain arising from lattice mismatch will also become an important and, in certain cases, a determining factor. In the absence of intentionally introduced shape and/or chemical anisotropy of the starting inorganic material (e.g., starting from nanorods with more reactive ends than sidewalls), different degrees of interfacial strain may lead to the following results. (1) When the crystal structures are compatible and the lattice parameters of the two crystalline phases are well-matched, core/shell (or nearly core/shell) structures usually arise.[5] (2) When there is a large lattice mismatch, interfacial strain may completely prevent heterojunction formation. (3) In special cases, where there

* Corresponding author. Phone: 217-333-7361. Fax: 217-333-2736. E-mail: mshim@uiuc.edu.

(1) (a) Gu, H.; Yang, Z.; Gao, J.; Chang, C. K.; Xu, B. *J. Am. Chem. Soc.* **2005**, *127*, 34. (b) Gu, H.; Zheng, R.; Zhang, X.; Xu, B. *J. Am. Chem. Soc.* **2004**, *126*, 5664. (c) Yu, H.; Chen, M.; Rice, P. M.; Wang, S. X.; White, R. L.; Sun, S. *Nano Lett.* **2005**, *5*, 379. (d) Mokari, T.; Rothenberg, E.; Popov, I.; Costi, R.; Banin, U. *Science* **2004**, *304*, 1787. (e) Kudera, S.; Carbone, L.; Casula, M. F.; Cingolani, R.; Falqui, A.; Snoeck, E.; Parak, W. J.; Manna, L. *Nano Lett.* **2005**, *5*, 445. (f) Choi, S.-H.; Kim, E.-G.; Hyeon, T. *J. Am. Chem. Soc.* **2006**, *128*, 2520. (g) Pellegrino, T.; Fiore, A.; Carlino, E.; Giannini, C.; Cozzoli, P. D.; Ciccarella, G.; Respaud, M.; Palmirotta, L.; Cingolani, R.; Manna, L. *J. Am. Chem. Soc.* **2006**, *128*, 6690. (h) Lu, Y.; Xiong, H.; Jiang, X.; Xia, Y.; Prentiss, M.; Whitesides, G. M. *J. Am. Chem. Soc.* **2003**, *125*, 12724.

(2) (a) Alivisatos, A. P. *Nat. Biotechnol.* **2004**, *22*, 47. (b) Wang, D. Y.; Rogach, A. L.; Caruso, F. *Nano Lett.* **2002**, *2*, 857.

(3) (a) Chen, M.; Kim, J.; Liu, J. P.; Fan, H.; Sun, S. *J. Am. Chem. Soc.* **2006**, *128*, 7132.(b) Smith, P. A.; Nordquist, C. D.; Jackson, T. N.; Mayer, T. S; Martin, B. R; Mbindyo, J.; Mallouk, T. E. *Appl. Phys. Lett.* **2000**, *77*, 1399. (c) Sharma, J.; Chhabra, R.; Liu, Y.; Ke, Y.; Yan, H. *Angew. Chem., Int. Ed.* **2006**, *45*, 730.

(4) (a) Balet, L. P.; Ivanov, S. A.; Piryatinski, A.; Achermann, M.; Klimov, V. I. *Nano Lett.* **2004**, *4*, 1485. (b) Kim, S.; Fisher, B.; Eisler, H.-J.; Bawendi, M. *J. Am. Chem. Soc.* **2003**, *125*, 11466.(c) Peng, P.; Milliron, D. J.; Hughes, S. M.; Johnson, J. C.; Alivisatos, A. P.; Saykally, R. J. *Nano Lett.* **2005**, *5*, 1809. (d) Erwin, S. C.; Zu, L.; Haftel, M. I.; Efros, Al. L.; Kennedy, T. A.; Norris, D. J. *Nature* **2005**, *436*, 91. (e) Dayal, S.; Krolicki, R.; Lou, Y.; Qiu, X.; Berlin, J. C.; Kenney, M. E.; Burda, C. *Appl. Phys. B: Lasers Opt.* **2006**, *84*, 309.

10.1021/cm0621390 CCC: $33.50
Published on Web 12/06/2006

is a large overall lattice mismatch but there exist coincidence site lattices between two crystalline materials under consideration, anisotropic structures (e.g., dimers where two nearly spherical particles are fused together with only one junction plane on each component) may be obtained.[6] As the size of the NCs becomes smaller, lattice-mismatch-induced strain may be relieved through processes such as surface relaxation. For example, the better accommodation of interfacial strain may explain the successful ZnS shell growth on small CdSe NCs but not on larger ones.[5]

In our previous report,[6] we have attributed the interface formation between iron oxide/II−VI semiconductor NCs leading to anisotropic heterostructures to the third scenario, where coincidence lattices[7] play an important role. However, even the most abundant (111)/(111) coincidence planes of inverse spinel iron oxide and CdS have a non-negligible mismatch of 4.4% on the basis of the bulk lattice parameters. Because the mismatch of the coincidence lattices is smaller than that in the CdSe/ZnS system where a core/shell type structure is formed, the (111)/(111) coincidence interface may be expected to be energetically favorable at small sizes. However, as the size of one or both components becomes larger, the build up of the lattice strain may lead to structural evolution and/or limitations (analogous to quantum dot formation via the Stranski−Krastanow mechanism in heteroepitaxy). In addition, the crystallinity and the crystal structure of the particles may vary at nanometer length scales, especially for iron oxides, which have several known crystalline phases. Here, we present studies on the effects of crystal structure, crystallinity, and crystallite size on the structural evolution of inverse spinel iron oxide/CdS colloidal NC heterostructures.

Experimental Section

Synthesis of Inverse Spinel Iron Oxide NCs. Standard airless techniques were used in all syntheses. Reagents were used as received. Inverse spinel iron oxide NCs were synthesized following ref 8.[8] Briefly, iron oxide NCs ~8 nm in diameter were synthesized by injecting 0.2 mL of $Fe(CO)_5$ into a solution containing 1.47 mL of oleic acid and 11 mL of octyl ether that was vacuum-degassed at 100 °C for at least 30 min. The reaction mixture was then refluxed at ~290 °C for 1 h. To synthesize iron oxide NCs ~5 nm (~12 nm) in average diameter, we used 0.98 mL (1.47 mL) of oleic acid and 7 mL (14 mL) of octyl ether. Chemically oxidized iron oxide NCs were synthesized by adding 0.34 g of $(CH_3)_3NO$ as described in ref 8.

Synthesis of Iron Oxide/CdS NC Heterostructures from S Powder and $Cd(acac)_2$. Iron oxide/CdS NC heterostructures were synthesized by direct addition of S powder and cadmium acetylacetonate [$Cd(acac)_2$] to the reaction mixture of iron oxide NCs as described previously.[6] Briefly, after S powder was added to the reaction flask containing iron oxide NCs at 100 °C, a solution of $Cd(acac)_2$, 1,2-hexadecanediol, and trioctylphosphine oxide (TOPO) in 1 mL of octyl ether was injected dropwise at 80 °C. The amount of S powder was varied as indicated. The amount of $Cd(acac)_2$ was adjusted to keep a molar equivalent of S powder. The amounts of 1,2-hexadecanediol and TOPO were both adjusted to be 3 mol equiv of S except for the two lowest Cd/S reagent concentration cases (conditions A and B indicated in Figure 4), for which they are kept at 4 mol equiv of S. After 10 min of stirring at 80 °C, the reaction mixture was heated to 280 °C and annealed for 30 min to 1 h. The final products were obtained by precipitating with ethanol and redissolving in chloroform. For studies on different average sizes of the initial iron oxide, the concentrations of Cd/S reagents are scaled by the inverse per NC volume ratio with respect to the condition that give rise to the highest yield of dimers for 7−8 nm diameter iron oxide (condition D in Figure 4). For example, 33 mg of S powder and 330 mg of $Cd(acac)_2$ were used for ~5 nm diameter iron oxide, which is 4.1 times (i.e., $(8\text{ nm}/5\text{ nm})^3$) the amounts used for the ~8 nm diameter case (8 mg of S powder and 80 mg of $Cd(acac)_2$).

Synthesis of Iron Oxide/CdS NC Heterostructures from Liquid Reagents. Appropriate amounts of 1 M trimethylsilyl sulfide (TMS_2S) in trioctylphosphine (TOP) as indicated were injected dropwise first to the reaction mixture of iron oxide NCs at 100−150 °C. One molar equivalent of dimethylcadmium (Me_2Cd) (1 M solution in TOP) was then added dropwise to the reaction mixture at 60 °C. After 10 min of stirring at 60 °C, the reaction mixture was heated to 280 °C and annealed for 1 h.

Characterization of Heterostructures of NCs. Transmission electron microscopy (TEM) samples were prepared with a dilute chloroform solution of NCs on Cu grids coated with thin carbon film (Tedpella Inc.). TEM analysis was carried out with JEOL 2010 LaB6 and JEOL 2010F both operating at 200 kV. Rigaku Geigerflex with a D-MAX system was used to acquire powder X-ray diffraction (XRD) patterns. Raman measurements were performed with a Jobin Yvon HR 800 micro-Raman spectrometer using 633 nm laser excitation. The laser power was 0.1 mW at the sample with a spot size of ~1 μm using a 100× objective. For laser-induced phase transformation, samples were exposed to a 15 mW laser with the same spot size. For both XRD and Raman measurements, all samples were transferred into a N_2-filled glovebox immediately following the reaction and all precipitation/redissolution was carried out using anhydrous solvents. Samples were prepared by drop casting a concentrated solution of NCs in chloroform on glass slides. The solvent was evaporated in vacuo, and the powder samples were sealed under a N_2 atmosphere.

Results and Discussion

Iron oxide has several well-known crystal structures. Because the synthesis of heterostrcutured NC colloids begins with the formation of iron oxide NCs, we first discuss the crystal structure and the crystallinity of the starting iron oxide NCs. Implications on the inorganic−inorganic interface formation and therefore on the overall morphology of heterostructured NC colloids are considered. We then discuss the size effect on the structural evolution of iron oxide/CdS NC heterostructures. The results of increasing the amounts of Cd/S reagents to examine the effects of increasing size of the CdS components on a fixed size of initial iron oxide NCs are presented first. The effects of the initial sizes of the presynthesized iron oxide NCs on the overall morphology of the anisotropic NC heterostructures are then presented.

(5) (a) Hines, M. A.; Guyot-Sionnest, P. *J. Phys. Chem.* **1996**, *100*, 468. (b) Dabbousi, B. O.; Rodriguez-Viejo, J.; Mikulec, F. V.; Heine, J. R.; Mattoussi, H.; Ober, R.; Jensen, K. F.; Bawendi, M. G. *J. Phys. Chem. B* **1997**, *101*, 9463. (c) Peng, X.; Schlamp, M. C.; Kadavanich, A. V.; Alivisatos, A. P. *J. Am. Chem. Soc.* **1997**, *119*, 7019. (d) Li, J. J.; Wang, Y. A.; Guo, W. Z.; Keay, J. C.; Mishima, T. D.; Johnson, M. B.; Peng, X. G. *J. Am. Chem. Soc.* **2003**, *125*, 12567.

(6) Kwon, K.-W.; Shim, M. *J. Am. Chem. Soc.* **2005**, *127*, 10268.

(7) (a) Bollmann, W. *Crystal Defects and Crystalline Interfaces*; Springer-Verlag: Berlin, 1970. (b) Brockman, A.; Balluffi, R. W. *Acta Metall.* **1981**, *29*, 1703. (c) Trampert, A.; Ploog, K. H. *Cryst. Res. Technol.* **2000**, *35*, 793.(d) Li, B. Q.; Zuo, J.-M. *Surf. Sci.* **2002**, *520*, 7.

(8) Hyeon, T.; Lee, S. S.; Park, J.; Chung, Y.; Na, H. B. *J. Am. Chem. Soc.* **2001**, *123*, 12798.

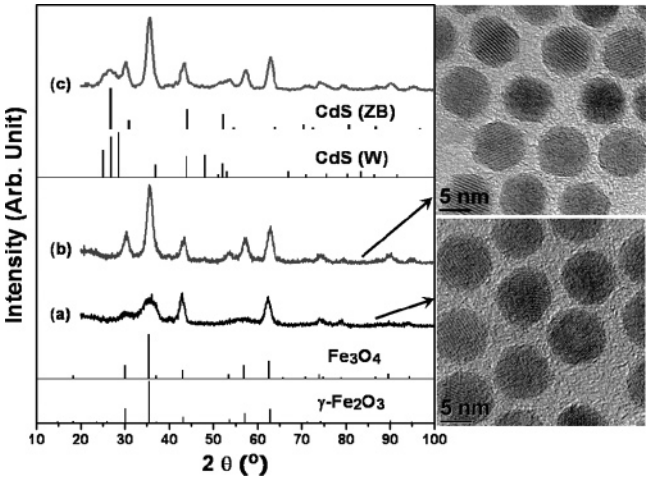

Figure 1. XRD and TEM images of (a) precursor iron oxide NCs without chemical oxidation prepared bythe method described in the experimental section, (b) "chemically oxidized" iron oxide NCs using $(CH_3)_3NO$, and (c) iron oxide/CdS NC heterostructures. The standard XRD patterns for γ-Fe_2O_3, Fe_3O_4, and wurtzite and zinc blende CdS were drawn from JCPDS files 00-039-1346, 00-019-0629, 03-065-2887, and 00-041-1049, respectively.

A. Crystal Structure and Crystallinity of the Initial Iron Oxide NCs. In the absence of oxidizing agents, thermal decomposition of $Fe(CO)_5$ is expected to lead to Fe(0), presumably in the amorphous or partially amorphous state. Iron oxide NCs used here are synthesized by thermal decomposition of $Fe(CO)_5$ in the presence of organic capping molecules and subsequent exposure to reagents for CdS formation. Many of the introduced reagents during the synthesis can lead to (partial) oxidation. Furthermore, similar iron oxide NC synthetic methods reported to date have led to different structures. Namely, both Fe_3O_4 and γ-Fe_2O_3 have been reported.[8,9] Therefore, we have first characterized the product of $Fe(CO)_5$ thermal decomposition in oleic acid and octyl ether (i.e., same conditions as NC heterostructure synthesis but prior to the addition of reagents for CdS growth) and then compared these results to those of NCs that have undergone intentional chemical oxidation via $(CH_3)_3NO$, which have been reported to lead to γ-Fe_2O_3.[8] We refer to the former as "precursor" iron oxide NCs and the latter intentionally oxidized NCs as "chemically oxidized."

Figure 1 shows the XRD patterns and the TEM images of the precursor and the chemically oxidized iron oxide NCs. The uppermost curve is the XRD pattern of iron oxide/CdS nanocrystal heterostructures. To be able to characterize, as closely as possible, the structure of the NCs in the reaction mixture, we have sealed samples inside a N_2-filled glovebox immediately following the synthesis to minimize undesirable postsynthesis oxidation in air, and the seal is broken only at the beginning of the XRD measurements. All three samples exhibit XRD patterns of inverse spinel iron oxide (Fe_3O_4 or γ-Fe_2O_3) crystal structure. The precursor NCs exhibit broader linewidths than both the chemically oxidized NCs and the heterostructures. The XRD peaks are expected to broaden with decreasing size of the crystallites and an average size can be estimated using the Debye−Scherrer equation.[10] However, iron oxide NCs in all samples are of similar sizes (7−8 nm), as shown in the TEM images for the presursor and chemically oxidized NCs. The narrowing of XRD peaks is then from the improved crystallinity rather than from increasing crystallite size.[11] The addition of Cd/S reagent and subsequent annealing step leads to crystallinity of iron oxide in NC heterostructures similar to that of chemically oxidized NCs.

Whereas the significant differences in the linewidths of XRD patterns help to identify that the iron oxide NCs are partially amorphous prior to CdS reagent addition, we cannot distinguish between Fe_3O_4 and γ-Fe_2O_3 from XRD measurements alone, because γ-Fe_2O_3 is a defective form of Fe_3O_4 (vacancies in the cation octahedral sites) and therefore nearly identical XRD patterns are observed for the two oxides. Raman spectroscopy has been a powerful tool in identifying various forms of iron oxides. Furthermore, Raman spectra have been obtained on samples that have been sealed inside a N_2 atmosphere and kept sealed during the measurements to minimize the effects of oxidation induced by air exposure. Figure 2a shows the Raman spectra of precursor iron oxide NCs ~7 nm in diameter. The bottom curve is obtained immediately after the synthesis on a sample that has been sealed in a N_2 atmosphere. The major feature is the relatively narrow peak at 670 cm^{-1} that corresponds to the A_{1g} mode of Fe_3O_4.[12a,b] The second and third curves from the bottom are obtained after breaking the seal and allowing the sample to be aerated. The gradual broadening via the appearance of the feature at ~700 cm^{-1} corresponds to the apppearance of γ-Fe_2O_3.[12b,c] The sample evolves from magnetite (Fe_3O_4) to maghemite (γ-Fe_2O_3) over time because of oxidation in air. As expected, both Fe_3O_4 and γ-Fe_2O_3 transform to the thermodynamically more stable hematite (α-Fe_2O_3) upon exposure to a high-intensity laser[12b,c] as shown in the uppermost curve in Figure 2a.

Raman spectra of chemically oxidized NCs are shown in Figure 2b. The average size of these NCs are ~8 nm, similar to the sample in Figure 2a. The bottom curve in Figure 2b corresponds to measurements on a sample that has been sealed in a N_2 atmosphere and kept sealed during the measurements. The upper curve is the same sample after aeration. Interestingly, chemical oxidation with $(CH_3)_3NO$ actually leads to Fe_3O_4, which converts to γ-Fe_2O_3 upon air-oxidation. The chemically oxidized NCs also undergo a transition to the α-phase upon irradiation with a high-intensity laser. In Figure 2c, Raman spectra of iron oxide/CdS NC heterostructures with an ~7 nm average diameter

(9) (a) Woo, K.; Hong, J.; Choi, S.; Lee, H.-W.; Ahn, J.-P.; Kim, C. S.; Lee, S. W. *Chem. Mater.* **2004**, *16*, 2814. (b) Casula, M. F.; Jun, Y.-W.; Zaziski, D. J.; Chan, E. M.; Corrias, A.; Alivisatos, A. P. *J. Am. Chem. Soc.* **2006**, *128*, 1675. (c) Peng, S.; Wang, C.; Xie, J.; Sun, S. *J. Am. Chem. Soc.* **2006**, *128*, 10676.

(10) Guinier, A. *X-Ray Diffraction: In Crystals, Imperfect Crystals, and Amorphous Bodies*; Freeman: San Francisco, CA, 1963.

(11) (a) Al Asmar, R.; Ferblantier, G.; Mailly, F.; Gall-Borrut, P.; Foucaran, A. *Thin Solid Films* **2005**, *473*, 49. (b) Kim, J. P.; Davidson, M. R.; Holloway, P. H. *J. Vac. Sci. Technol., B* **2003**, *21*, 2048. (c) Ferblantier, G.; Mailly, F.; Al, Asmar, R.; Foucaran, A.; Pascal-Delannoy, F. *Sens. Actuators, A* **2005**, *A122*, 184.

(12) (a) Shebanova, O. N.; Lazor, P. *J. Raman Spectrosc.* **2003**, *34*, 845. (b) de Faria, D. L. A.; Silva, S. V.; de Oliveira, M. T. *J. Raman Spectrosc.* **1997**, *28*, 873. (c) Varadwaj, K. S. K.; Panigrahi, M. K.; Ghose, J. *J. Solid State Chem.* **2004**, *177*, 4286.

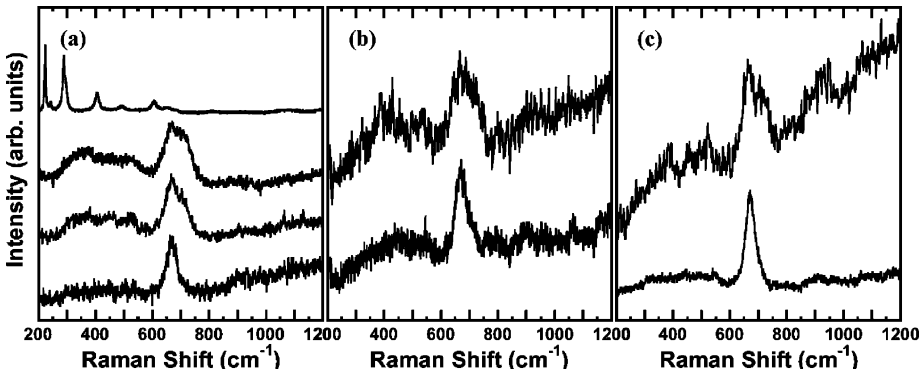

Figure 2. (a) Raman spectra of precursor iron oxide NCs without intentional chemical oxidation. From bottom to top curves: without air exposure (Fe_3O_4), after air exposure (Fe_3O_4 to γ-Fe_2O_3 transition), further air exposure (mainly γ-Fe_2O_3), and after 2 MW/cm^2 laser exposure (α-Fe_2O_3). Note that the transition to α-Fe_2O_3 can be observed at laser intensity >130 kW/cm^2. (b) Raman spectra of iron oxide NCs chemically oxidized without air exposure exhibiting Fe_3O_4 (bottom curve) and after air exposure exhibiting mainly γ-Fe_2O_3 (top curve). (c) Raman spectra of iron oxide/CdS heterostructures without air exposure exhibiting Fe_3O_4 (bottom curve) and after air exposure exhibiting mainly γ-Fe_2O_3 (top curve). All measurements were conducted at low laser intensity, as indicated in the text.

iron oxide component are shown. The bottom curve corresponds to a sample sealed in a N_2 atmosphere and kept sealed during the measurements. Again, the A_{1g} mode at 670 cm^{-1} indicates that the iron oxide is predominently Fe_3O_4.[12a,b] Similar to both the precursor and the chemically oxidized iron oxide NCs, there is a transition to γ-Fe_2O_3 with air exposure and to α-Fe_2O_3 upon high-intensity laser exposure. It is interesting to note that the epitaxial attached CdS does not alter the transformation of Fe_3O_4 to γ-Fe_2O_3 as well as laser-induced transformation to α-Fe_2O_3. We also note that in all three cases, the air-induced Fe_3O_4 to γ-Fe_2O_3 transition seems to continue over several weeks to months at room temperature.

The above observations indicate the following about the nature of iron oxide NCs during the synthesis of anisotropic NC heterostructures. Prior to Cd/S reagent addition, NCs are predominently Fe_3O_4 and partially amorphous. Annealing at elevated temperatures with Cd/S reagents leads to increased crystallinity of Fe_3O_4 NCs. Only after the postsynthesis air exposure is there a conversion of Fe_3O_4 to γ-Fe_2O_3. We note that our previous assignment of γ-Fe_2O_3 in NC heterostructures was made on the basis of air-exposed samples.[6] Whereas we now assign Fe_3O_4 to the as-synthesized NC heterostructures on the basis of the above Raman measurements, our treatment of coincident junction planes and the interfacial lattice strain remains the same, because the two forms of iron oxides have inverse spinel structure with essentially identical lattice parameters. Although the iron oxide components eventually convert to γ-Fe_2O_3, we refer to the iron oxide component as Fe_3O_4 for the remainder of this paper for simplicity. The partially amorphous Fe-rich oxide NCs are likely to aid the initial adsorption of S, which in turn promotes surface heterogeneous nucleation rather than isolated homogeneous nucleation of CdS, consistent with our previous obsrevation[6] that CdS growth on chemically oxidized NCs (which are also more crystalline) leads to a significantly reduced yield of heterointerfaces. However, this incomplete crystallinity leads to a question of whether CdS is epitaxially grown on the initial Fe_3O_4 NCs or further crystallization of the initial oxide is induced after crystalline CdS has already formed (and therefore Fe_3O_4 orients with respect to CdS). This question is addressed in the following sections as we discuss how the overall structure of NC heterojunction colloids evolves with CdS content and the initial Fe_3O_4 NC size.

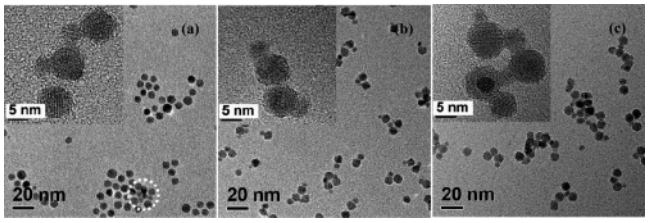

Figure 3. TEM images of Fe_3O_4/CdS NC heterostructures synthesized from (a) low concentration, (b) intermediate concentration, and (c) high concentration of Cd/S reagents. The amounts of Cd/S reagents in (a−c) correspond to conditions A, D, and F in Figure 4, respectively. Heterostructures are circled in (a). The insets are high magnification images.

B. Structural Evolution with Increasing CdS Content. In an attempt to examine how increasing the size of the CdS component affects the morphology of the heterostructured NCs, we have first extended our previous approach using S powder and Cd(acac)$_2$ simply by increasing the amount of these reagents added to a fixed size and concentration of Fe_3O_4 NCs. However, the initial aggregation of NCs upon S powder addition complicates the situation. These results from S-powder-based synthesis are discussed first. To circumvent this aggregation issue, we have extended the synthesis utilizing liquid reagents, namely, TMS_2S and Me_2-Cd, and a discussion on the results of these studies follows.

S-Powder-Based Synthesis. TEM images of NC heterostructures obtained with increasing amount of Cd/S reagents are shown in Figure 3. In the lowest concentration (Figure 3a), many particles are isolated Fe_3O_4 NCs, as expected, but there are also a significant number of dimers (~18%) and oligomers (~6%). In the intermediate case (Figure 3b), dimers are predominant (~51%). At higher concentrations (Figure 3c), similar yields of isolated particles (~34%), dimers (~33%), and oligomers (~33%) are observed. We refer to any NCs that have three or more particles fused together as oligomers. In all conditions examined, the predominant interfaces are (111)/(111) with aligned zone axes, consistent with our previous report.[6]

Different amounts of S powder and Cd(acac)$_2$ to synthesize Fe_3O_4/CdS heterostructures for a fixed size (7−8 nm) of

Fe_3O_4 NCs are labeled A through F in Figure 4. TEM images in Figure 3a−c correspond to conditions A, D, and F, respectively. Condition D (0.25 mmol of each reagent or 8 mg of S powder and 80 mg of $Cd(acac)_2$) is the amounts of Cd/S reagents that lead to the highest yield of dimers (∼51%).[6] The amounts of S and $Cd(acac)_2$ are varied from 1/8 to twice the amounts used in this condition. The relative yields of isolated particles, dimers, and oligomers are shown for different reaction conditions in Figure 4. The yields for each type of particles are obtained on the basis of more than 300 NCs counted from TEM images for each reaction condition. As the amount of Cd/S reagents increases, the yield of isolated particles decreases from ∼77 to ∼20% until condition D but then increases slightly to ∼35% with higher Cd/S reagent amounts. This trend of initial decrease followed by an increase can be explained by the fact that at low Cd/S reagent concentrations, the majority of the isolated particles are Fe_3O_4, whereas a significant amount of isolated CdS NCs begin to be nucleated at high Cd/S reagent concentrations. The relative abundance of dimers peaks at condition D, whereas the oligomer yield increases monotonically. Although the increase in relative yields of oligomers upon increasing the Cd/S reagents may be expected, interestingly, the average size of the CdS component remain essentially constant. The average size of CdS component synthesized at the lowest concentration of Cd/S reagents (condition A) is 4.6 nm, whereas the average size is 4.7 nm in the highest concentration case (condition F). This is in contrast to the expectation based on thermodynamic driving force to minimize the surface-to-volume ratio.

The limited size of CdS may be explained by the build up of lattice strain. That is, beyond a certain size, there is too much lattice strain such that growth stops and the nucleation of new particles is favored. However, the situation with solid S reagent becomes complicated because of the initial partial aggregation of NCs. Note that in Figure 3c, oligomers consist of multiple Fe_3O_4 NCs interconnected by CdS NCs. We suspect that this is the result of the initial S-induced aggregation. This aggregation of NCs is an advantage in that it prevents or minimizes separate homogeneous nucleation of CdS. but the high local Cd/S reagent concentration for all conditions makes it difficult to conclude whether or not the build up of lattice strain limits the size of CdS component. Therefore, we have examined a synthetic route that utilizes liquid reagents as discussed below.

Liquid Cd/S Reagent-Based Synthesis. Figure 5a−d shows TEM images of Fe_3O_4/CdS NC heterostructures synthesized using different amounts of TMS_2S and Me_2Cd. All syntheses start with similarly sized (7−8 nm) Fe_3O_4 NCs, and the predominant interface in the heterostructures is again (111)/(111) with aligned zone axes. In Figure 5e, the distributions of isolated particles, dimers, and oligomers for each concentration of TMS_2S and Me_2Cd are shown. In the lowest concentration of TMS_2S and Me_2Cd (0.05 mmol of each in the reaction mixture), heterostructures with very small (∼2 nm) CdS are observed, as shown in Figure 5a. Isolated particles observed are all individual Fe_3O_4 NCs in this case. Increasing the concentration of TMS_2S and Me_2Cd leads to a slight increase in CdS particle size in heterostructures and

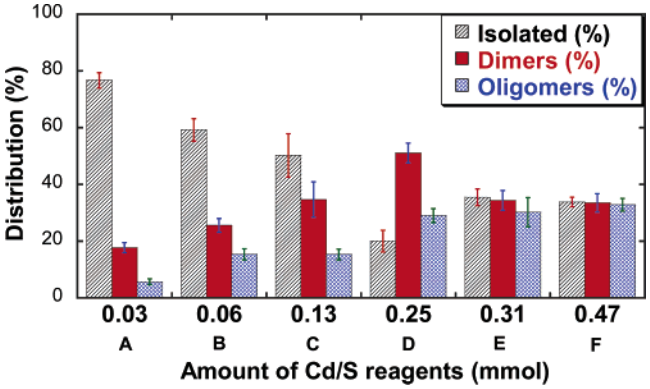

Figure 4. Distribution of isolated particles/dimers/oligomers for different amounts of $Cd(acac)_2$/S powder. Cd and S reagents are 1:1 molar ratio in all cases.

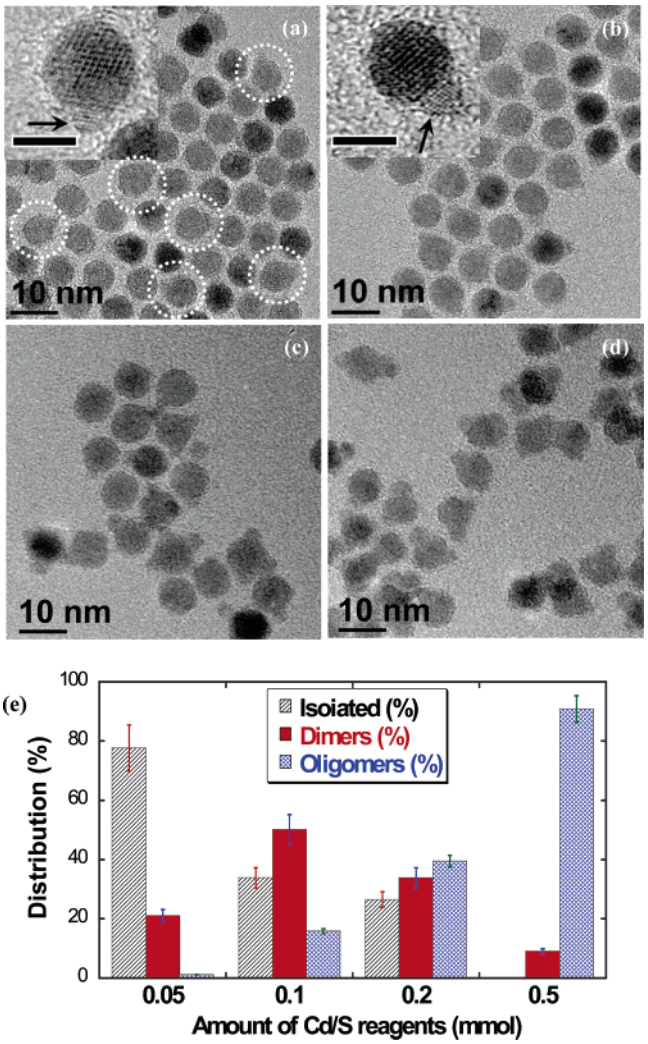

Figure 5. TEM images of Fe_3O_4/CdS NC heterostructures synthesized using (a) 0.05, (b) 0.1, (c) 0.2, and (d) 0.5 mmol each of TMS_2S and Me_2Cd. (e) Distribution of isolated particles/dimers/oligomers for different amounts of Me_2Cd/TMS_2S. Heterostructures are circled in (a). The arrows in the insets of (a) and (b) point to the CdS component. Scale bars in the insets are 5 nm.

essentially no isolated individual particles. Figure 6 compares the average size of CdS particles in NC heterostructures from S-powder-based and liquid-reagent-based syntheses. In the S powder synthesis, the size of CdS particles remains constant; this is most likely due to partial aggregation, which causes a high local concentration of Cd/S reagents, even in

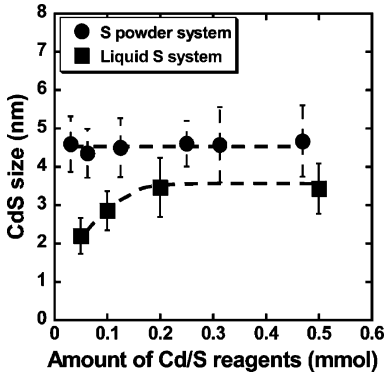

Figure 6. Size of CdS in heterostructures for different amounts of Cd/S reagents using $Cd(acac)_2$/S powder (circles) and Me_2Cd/TMS_2S (squares). Lines are guides for the eyes.

the low concentration limit studied here. However, in the liquid reagent synthesis, there is a noticeable increase at low concentrations and the structures approach a (slightly smaller) size similar to that in the S powder synthesis in the high concentration limit.

The most striking difference between the S powder approach and the liquid-reagent-based synthesis is that the oligomers in S-powder-based approach consist of multiple NCs of both types, whereas essentially all oligomers observed in the liquid reagent synthesis have only a single Fe_3O_4 NC. This difference may be explained by the fact that the S powder addition induces initial partial aggregation of Fe_3O_4 NCs. This complication prevents us from analyzing how increasing the size of CdS affects the morphology of the heterostructured colloids. The liquid-reagent-based synthesis circumvents this complication and reveals that multiple CdS particle nucleation rather than continued growth of CdS occurs upon increasing the amount of Cd/S reagents. The maximum size of CdS NCs observed in heterostructures with 7−8 nm Fe_3O_4 NCs is ∼4 nm in the liquid reagent synthesis. This size is similar to the size of CdS particles observed in all concentrations examined with S-powder-based synthesis, for which we anticipate the local concentration of Cd/S reagents to be fixed because of the aggregation of Fe_3O_4 NC upon S powder addition. Our observation of the initial increase in CdS size at low concentrations followed by multiple particle nucleation rather than continued growth in the liquid-reagent-based synthesis is consistent with the idea that the size of CdS particles is limited by the built up lattice strain.

C. Structural Evolution with Increasing Initial Fe_3O_4 NC Size. To examine this potential effect of lattice-strain-induced size limit further, we now discuss how the initial size of the Fe_3O_4 NCs alters the overall morphology. Similar to all previous cases, (111)/(111) interfaces with aligned zone axes are the largest number of heterojunctions observed for all sizes of starting Fe_3O_4. TEM images of Fe_3O_4/CdS heterostructures with different sizes of Fe_3O_4 are shown in Figure 7a−c. Both ∼5 and ∼8 nm diameter Fe_3O_4 NCs lead to predominantly dimer type heterostructures. However, there is a striking difference between the two cases. The smaller Fe_3O_4 NCs lead to heterostructures that have a significantly larger CdS component. The heterostructures consist of ∼8−12 nm diameter CdS particles when the initial Fe_3O_4 is ∼5 nm, as opposed to a maximum CdS size of 4−5 nm for the larger ∼8 nm Fe_3O_4. When the size of the initial Fe_3O_4 is increased further to ∼12 nm, the maximum size of the CdS component remains at ∼4 nm.

These observations may be explained by considering that smaller NCs can relieve or accommodate interfacial strain more effectively. When the size of the initial Fe_3O_4 NCs is small, CdS can nucleate and grow to relatively large sizes, as exemplified in Figure 7a, where CdS grows to be about twice as large as the initial Fe_3O_4 NCs. Increasing the size of the Fe_3O_4 NCs limits the maximum growth size of the CdS component due to lattice strain. Increasing the amount of Cd/S reagents leads to additional nucleation of CdS particles rather than continued growth of existing particles because of this limitation. Combined with the fact that the junction planes exhibit preferred orientation of coincidence planes, these observations are consistent with lattice-strain-

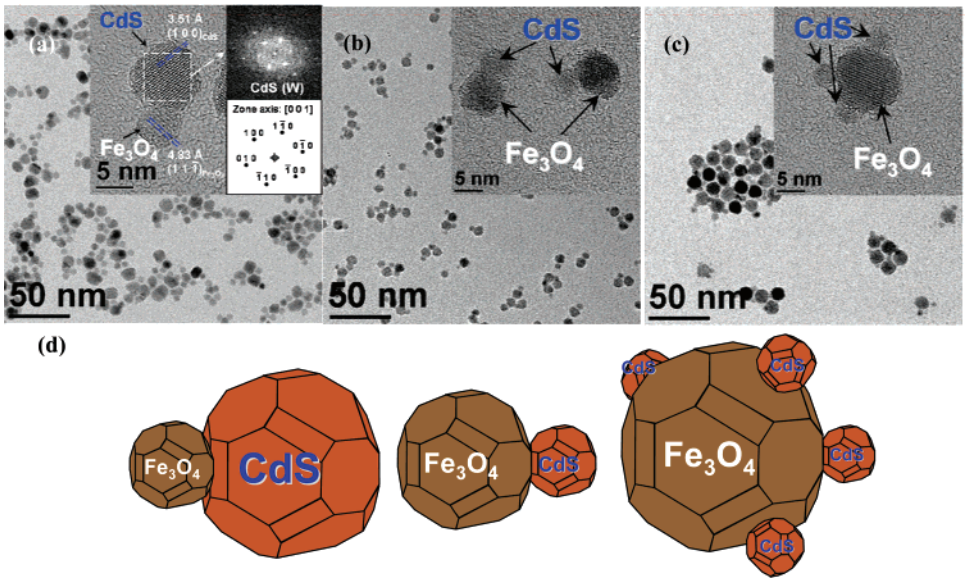

Figure 7. TEM images of NC heterostructures consisting of (a) ∼5 nm Fe_3O_4/8−12 nm CdS, (b) ∼8 nm Fe_3O_4/4−5 nm CdS, and (c) ∼12 nm Fe_3O_4/2−4 nm CdS. Insets are corresponding higher magnification images. Inset of (a) also shows the FFT pattern obtained from the larger particle, indicating it to be wurtzite CdS. (d) Schematic of structural evolution of heterostructures with the initial size of Fe_3O_4 NCs.

induced size limits and suggest that CdS grows epitaxially on Fe_3O_4, even if the initial Fe_3O_4 NCs are partially amorphous.

Conclusion

We have shown that the size of NCs is a critical factor in determining how the morphology of NC heterostructures evolves. The studies carried out here help to elucidate the mechanism of heterojunction formation, which in turn is necessary in developing rational and controllable approaches to synthesizing NC-based multifunctional materials. Combined Raman and XRD measurements have revealed that the initial iron oxide NCs are partially amorphous magnetite (Fe_3O_4) that eventually convert to γ-Fe_2O_3 upon exposure to air. Reaction conditions for forming heterojunctions with CdS lead to improved crystallinity of Fe_3O_4 NCs. Increasing the amount of Cd/S reagents in an attempt to examine how a larger size of CdS affects the heterostructure morphology has revealed that lattice strain is likely to be limiting the maximum size of CdS that can be obtained in these heterostructures. For Fe_3O_4 NCs with diameters larger than ~7 nm, lattice strain prevents CdS growth beyond ~4 nm and the addition of excess Cd/S reagents leads to multiple CdS particle nucleation on individual Fe_3O_4 NCs. Reducing the size of the initial Fe_3O_4 NCs allows epitaxial growth of significantly larger CdS NCs. These results demonstrate the possibility of engineering multicomponent NC heterostructures with nanometer precision by exploiting lattice strain induced by heterointerfaces.

Acknowledgment. This material is based on work supported by the NSF (Grant DMI-0322299) and the U.S. Department of Energy, Division of Materials Sciences, under Award DEFG02-91-ER45439, through the Frederick Seitz Materials Research Laboratory at the University of Illinois at Urbana−Champaign. Part of the research for this publication was carried out in the Center for Microanalysis of Materials, University of Illinois at Urbana−Champaign, which is partially supported by the U.S. Department of Energy under Grant DEFG02-91-ER45439.

CM0621390